Nup107 is a crucial regulator of Torso-mediated metamorphic transition in *Drosophila melanogaster*

Jyotsna Kawadkar[1*] and Ram Kumar Mishra[1*]

Department of Biological Sciences, Indian Institute of Science Education and Research (IISER) Bhopal

* Corresponding author(s): jyotsna19@iiserb.ac.in, rkmishra@iiserb.ac.in

Abstract

The holometabolous metamorphosis in *Drosophila* is governed by neuropeptide hormone signaling, culminating in the surge of 20-hydroxyecdysone levels and ecdysone receptor signaling. Nucleoporins (Nups) form nuclear pore complexes, influencing nucleocytoplasmic transport, cell division, and gene regulation. The Nup107-160 complex (Y-complex) members have been studied in disease and organism development, and we have explored the role of Nup107 in *Drosophila* development.

Here, we report a unique regulation exerted by the Nup107 in metamorphic transition during *Drosophila* development. *Nup107* depletion induces developmental arrest in third-instar larvae, impeding tissue growth and a complete cessation of pupariation. This lack of pupariation is due to the loss of EcR nuclear translocation and inhibited downstream transcriptional activation. We argue that Nup107 modulates the EcR activation pathway by controlling the ecdysone biosynthesis, as *Nup107* depletion negatively impacts the transcription of the Halloween genes. Feeding ecdysone to *Nup107*-depleted larvae restores normal EcR signaling and metamorphosis. Overexpression of the receptor tyrosine kinase, *torso*, and MAP-kinase pathway activator, *ras*, in

Nup107 depletion background rescued the developmental delay phenotypes. Through our observations, we propose that Nup107 is a key regulator of Torso-mediated activation of EcR signaling required for the ecdysone at larval to pupal metamorphic transition in *Drosophila*.

Introduction

The Nuclear pores are a multi-protein assembly of nucleoporins (Nups), and they orchestrate molecular trafficking between the nucleus and the cytoplasm in eukaryotic cells. Nuclear pores are embedded in the nuclear membrane and have an approximate molecular mass of 110 megadaltons (Hetzer and Wente 2009; Hoelz et al. 2016). Decades of detailed analysis using electron microscopy have provided comprehensive insights into the architecture of nuclear pore complexes (NPCs). NPCs present a symmetric core characterized by eight-fold rotational symmetry along the nucleocytoplasmic axis. Proteomic analyses conducted in yeasts and vertebrates have contributed to our understanding of NPC composition, revealing that it is constituted of approximately 30 distinct proteins collectively referred to as nucleoporins (Rout et al. 2000; Cronshaw et al. 2002). The NPC consists of three primary substructures: the outer cytoplasmic and inner nuclear rings, which surround a central inner ring called the scaffold ring, primarily aiding in the process of nucleocytoplasmic transport (Lin and Hoelz 2019).

The outer ring of the NPC scaffold comprises the largest Nup107 complex, also called the Y-complex. In metazoans, Y-complex is composed of ten distinct subunits (ELYS, Nup160, Nup133, Nup107, Nup96, Nup85, Nup43, Nup37, Sec13, and Seh1), with ELYS being a sub-stoichiometric member (D'Angelo and Hetzer 2008; Morchoisne-Bolhy et al. 2015). Nup107 forms the stalk of the Y-complex and is one of the lead determinants of Y-complex stability. The Nup107 complex

plays a pivotal role in facilitating ELYS-coordinated post-mitotic NPC assembly (Boehmer et al. 2003; Walther et al. 2003) and messenger RNA (mRNA) export (Bai et al. 2004). Additionally, it actively participates in mitosis, contributing to the regulation of kinetochore-microtubule polymerization (Zuccolo et al. 2007; Mishra et al. 2010). The multitude of Y-complex functions underscores its critical importance in various cellular processes, serving as a central component in maintaining cellular homeostasis.

While Nups largely remain permanently associated with NPC, specific cellular conditions may demand dynamic behaviors from Nups. This may signify their involvement in processes other than nucleo-cytoplasmic transport and their ability to associate with the NPC transiently (Rabut et al. 2004a; Rabut et al. 2004b). As a stable constituent of NPC, Nups are associated with chromatin and exert transcriptional regulation. Notably, interactions between active genes and Nups occurring predominantly within the nucleoplasm have been reported for dynamic Nups such as Nup98, ELYS, and Sec13 (Capelson et al. 2010b; Kalverda et al. 2010; Kuhn et al. 2019). ELYS, a Nup and also a transcription factor, governs *Drosophila* development. *ELYS* RNAi results in developmental defects owing to the reactivation of the Dorsal (NF-κB) pathway during late larval stages (Mehta et al. 2020).

Nup107 is an indispensable component of the Y-complex, and at the nuclear periphery, it is associated with genes that undergo active transcription (Gozalo et al., 2020). The disruption of Nup107 in zebrafish embryos leads to significant developmental anomalies, including the absence of the pharyngeal skeleton, swim bladder, and diminished eye size (Zheng et al. 2012). A thorough analysis of biallelic Nup107 mutations (D157Y, D831A) correlates well with clinical conditions such as microcephaly and Steroid-resistant nephrotic Syndrome (Miyake et al. 2015). Nup107 appears to significantly influence the regulation of cell fate in aged and transformed cells by

modulating EGFR signaling and the nuclear trafficking of ERK protein (Kim et al. 2010). In *Drosophila*, Nup107 co-localizes with Lamin during meiotic division, and Nup107 depletion perturbs lamin localization, leading to a higher frequency of cytokinesis failure in male meiosis (Hayashi et al. 2016). Knockdown of *Nup107* in the somatic cells of the gonad (gonadal soma) produces ovarian-dysgenesis-like phenotypes, and transcriptomic analysis identifies the somatic sex-determination gene *doublesex* (*dsx*) as a target of Nup107 (Weinberg-Shukron et al. 2015; Shore et al. 2022). Collectively, these findings delineate the multifaceted roles of Nup107 in diverse cellular processes, ranging from development to meiotic division and somatic sex determination.

During development, *Drosophila* undergoes elaborate metamorphosis during larvae to mature adult transition. Metamorphosis is initiated by the neuropeptide prothoracicotropic hormone (PTTH) produced from neurons in the larval brain (Rewitz et al. 2013). In the prothoracic gland (PG), the primary insect endocrine organ, PTTH signals through the receptor tyrosine kinase (RTK) Torso. The RTK signaling activates the MAP-kinase pathway, thereby triggering the production and release of ecdysone hormone. However, ecdysone synthesis can be regulated by other signaling pathways, such as the EGFR pathway (Yamanaka et al. 2013; Cruz et al. 2020), and the mechanism of some of these processes awaits elucidation. We selected *Drosophila melanogaster* (fruit flies) as the model organism to elucidate the significance of Nup107 in metamorphosis.

In a reverse genetic RNAi screening for Y-complex members, we noted that *Nup107* RNAi induces a significant developmental arrest at the third instar larval stage. Further analysis revealed that the Ecdysone Receptor (EcR) signaling pathway is perturbed, and EcR fails to translocate into the nucleus in *Nup107* knockdown. The failure of the EcR nuclear localization upon *Nup107* depletion

is due to the diminished ecdysone hormone levels during the late third instar larval stage. EcR pathway disruption impacts the neuroendocrine axis, which is responsible for triggering the pupariation-inducing ecdysone surge and consequently influencing the timing of maturation. We reasoned that the prominent RTK pathway downstream of the Torso may be affected. In accordance, overexpression of the *torso* and the ras^{V12} in *Nup107* depleted larvae rescued the developmental arrest and subsequently initiated pupation. In summary, our observation emphasizes novel regulatory functions for Nup107 in torso-mediated metamorphosis. We propose that Nup107, a key regulator of torso-pathway activation in the PG, enables ecdysone surge for efficient metamorphic transition.

Results

Nup107 is essential for larval to pupal metamorphosis

Analysis of Nup107 in the mammalian cell culture system has shed light on critical regulatory roles in vertebrates, yet its importance in development is poorly understood. In this context, we started the characterization of *Drosophila* Y-complex member Nup107 in greater detail. Utilizing RNAi lines ($Nup107^{KK}$ and $Nup107^{GD}$), we performed ubiquitous depletion through *Actin5C-GAL4*. Interestingly, *Nup107* depletion, leading to larvae arrest at the third instar stage, was accompanied by an extension of larval feeding and growth periods, causing complete cessation of pupariation (Fig. 1A-A'). Quantitative assessment of *Nup107* transcript levels in the $Nup107^{GD}$ and $Nup107^{KK}$ RNAi lines suggested approximately 30-40% knockdown (Fig. 1B). Polyclonal antibodies were raised against the Nup107 amino-terminal antigenic fragment (amino acids 1–210, see methods for details). Purified anti-Nup107 antibodies detected a band of approximately

~100kDa in lysates prepared from the control larval brain complex. When Nup107 antibodies were used on similar lysates prepared from ubiquitous *Nup107* knockdown organisms (*Actin5C-GAL4* driving *Nup107* RNAi, denoted as ubiquitous hereon), the band intensity was significantly reduced (Fig. 1C). Further, the immunostaining with Nup107 antibodies identified a conserved and robust nuclear rim staining pattern in salivary gland tissues, overlapping with mAb414 antibodies recognizing FG-nucleoporins in nuclear pores (Supplemental Fig. S1E-H). We also examined the localization of the Nup107 antibody in conjunction with mRFP-tagged *Nup107* expressed through its endogenous promoter (Supplemental Fig. S1A-D). These observations confirm the efficacy of *Nup107* knockdown and provide a handle to assess levels and localization of Nup107 in affected tissues. To further investigate the role of Nup107 in development, we generated a *Nup107* null mutant using CRISPR-Cas9-mediated gene editing. The mutant, targeting regions close to the start and stop codon of the *nup107* gene, was confirmed by PCR and sequencing (Supplemental Fig. S2A, B). However, the $Nup107^{KO}$ is homozygous lethal at the embryonic stage, prompting us to continue our studies with the *Nup107* RNAi line. This comprehensive approach involving RNAi-mediated knockdown and CRISPR-Cas9 gene editing provides valuable insights into the significance of *Nup107* in *Drosophila* development.

Nup107 **contributes significantly to ecdysone signaling**

In our investigation, the depletion of *Nup107* in *Drosophila* larvae resulted in an extension of the feeding and growth period, ultimately leading to developmental arrest at the third instar stage. In contrast to wild-type larvae progressing into pupation, *Nup107* knockdown larvae exhibited a distinct halt in development, as depicted in Fig. 1A'. To discern the pathways governing the onset of maturation, we focused on the juvenile to adult developmental transition in *Drosophila*, a process primarily triggered by elevated levels of the sole insect steroid hormone, ecdysone (the

active form is 20-hydroxyecdysone, 20E). Ecdysone production in the PG is stimulated by PTTH, a neuropeptide secreted by bilateral neurons projecting into PG (McBrayer et al. 2007; Johnson et al. 2013; Shimell et al. 2018). PTTH initiates ecdysone production, and subsequently, ecdysone is released into the circulatory system, where it is converted into its active form, 20E, by peripheral tissues. The 20E steroid operates through the nuclear receptor, the ecdysone receptor. Upon binding to its receptor, the complex translocates into the nucleus, which binds to chromatin, activating ecdysone-induced genes (Kozlova and Thummel 2002; Johnston et al. 2011; Tennessen and Thummel 2011).

In our investigation, we examined the localization of EcR in the late third instar salivary glands of both control and *Nup107*-depleted larvae (using the *Nup107*^{KK} line). Intriguingly, we observed that *Nup107* depletion hindered the translocation of EcR into the nucleus, retaining it in the cytoplasm. In contrast, wild-type larvae exhibited EcR localization within the nucleus (Fig. 2A-J). Quantitative analysis of EcR intensities in the cytoplasm and nucleus further underscored a significant decrease in EcR signals inside the nucleus when *Nup107* is depleted (Fig. 2K). This observation further emphasizes that the Nup107 is required for EcR nuclear localization to mediate critical larval to pupal developmental transition. Furthermore, we observed that the organ size (salivary glands and the brain complex) in *Nup107* depleted larvae is significantly smaller (Supplemental Fig. S3).

Prompted by the cytoplasmic accumulation of EcR, we investigated whether the mRNA levels of ecdysone-inducible genes were affected. When 20E binds with EcR, the activated EcR with enhanced affinity occupies the ecdysone response element (ERE) region in gene promoters. The ecdysone receptor is thought to function in a positive auto-regulatory loop, which may elevate EcR levels and sustain ecdysone signaling (Varghese and Cohen 2007). Firstly, we examined the EcR

transcript levels, revealing a reduction under *Nup107* depletion conditions (Fig. 2L). Subsequently, we measured the mRNA levels of known *EcR* target genes, *Eip75A* and *Eip74EF*, finding that the expression of each target reduced in correlated *Nup107* knockdown levels (Fig. 2M, N). Similar results were observed in the depletion of *Nup107* using the GD-based RNAi line (Supplemental Fig. S4). The defects observed during metamorphic transitions can be attributed to impaired ecdysone signaling upon *Nup107* depletion, which prompted a closer examination of their regulatory relationship.

Nup107 **does not directly contribute to EcR nuclear import in the target tissue**

We established in Fig. 2 that the nuclear localization of EcR is impaired upon *Nup107* knockdown. Typically, EcR nuclear localization follows an intricate mechanism where 20E binding to EcR allows its nuclear translocation and subsequent activation of its target genes (Cronauer et al. 2007; Johnston et al. 2011; Lenaerts et al. 2019). Thus, the prothoracic gland, responsible for producing ecdysone hormone from dietary cholesterol through a process involving a group of P450 enzymes coded by the Halloween genes, is indispensable for EcR activation (Niwa and Niwa 2014; Kannangara et al. 2021). Notably, the efficient nuclear import of MAD transcription factor is affected by several Y-complex members, including Nup107 (Chen and Xu 2010). Moreover, nucleoporins were reported to facilitate nuclear transport of Met juvenile hormone receptors (He et al. 2017). Consequently, we posited the hypothesis that Nup107 may regulate active 20E-EcR complex formation through 20E in ubiquitous *Nup107* knockdown or directly regulate EcR nuclear import in the target tissue.

To address this hypothesis, we chose salivary glands to see if the nuclear import of EcR is affected when *Nup107* is depleted using salivary glands-specific *AB1-GAL4* and PG-specific *Phm-GAL4*. Surprisingly, in contrast to the ubiquitous knockdown of *Nup107*, nuclear localization of EcR

remained unaffected in salivary gland-specific *Nup107* knockdown (Fig. 3A-J; Supplemental Fig. 6A-J). However, the PG-specific knockdown phenocopied the nuclear localization defects of EcR (Fig. 3K-O; Supplemental Fig. 6K-O). Further, the PG-specific knockdown induced an extended third instar stage lifespan (10-12 days after egg laying, Supplemental Fig. 5B, B', C). Quantification of EcR signals from cytoplasm and nucleus of *Nup107* depleted late third instar salivary gland cells and comparison with control salivary glands indicates that the nuclear/cytoplasmic ratios are drastically reduced in case of PG-specific depletion, but unaltered in salivary gland-specific *Nup107* depletion (Fig. 3P; Supplemental Fig. 6P). In accordance with unperturbed EcR nuclear translocation, salivary glands-specific depletion of *Nup107* yielded no discernible differences in larval growth and pupariation compared to the control (Supplemental Fig. 5A, A', C). Consistent with these observations, expression levels of ecdysone-inducible genes *Eip75* and *Eip74EF* were significantly reduced in PG-specific *Nup107* knockdown (Fig. 3Q, R). The observed decrease in ecdysone-inducible gene expression during late third-instar developmental stages can explain the potential impairment of metamorphosis induction seen upon ubiquitous or PG-specific *Nup107* knockdown. In addition to the salivary gland and brain complex, we also noticed a compromise in the size of the Prothoracic Gland upon *Nup107* knockdown (Supplemental Fig. S7).

These observations suggest that Nup107 exerts a regulation on ecdysone bioavailability and active 20E-EcR complex formation rather than a direct role in EcR nuclear translocation. Nup107 can also directly regulate the 20E biosynthesis.

Nup107 **exerts control on the EcR pathway through Ecdysone level regulation**

We reasoned that Nup107 may regulate the ecdysone biosynthesis in PG to impact the larval arrest. We delved into analyzing the effect of *Nup107* knockdown on ecdysone production. The

considerable decrease in PG size due to *Nup107* knockdown (Supplemental Fig. S7) may contribute to the reduced 20E levels. This prompted us to explore the potential role of Nup107 in influencing ecdysone production, and we assessed the impact of *Nup107* knockdown on ecdysone biosynthesis.

Utilizing an ELISA-based detection method, we assessed 20E levels in larvae at 96 hours and 120 hours after egg laying (AEL). Larvae from different experimental conditions, including control, ubiquitous *Nup107* depletion, and PG-specific *Nup107* depletion, were used in this analysis. Strikingly, the results indicated a substantial decrease in total 20E levels upon *Nup107* knockdown (Fig. 4A; Supplemental Fig. S8A), particularly 120 AEL coinciding with the 20E surge seen during metamorphosis. This observation suggested a potential defect in ecdysone biosynthesis when *Nup107* is depleted.

The Prothoracicotropic hormone signaling from the brain to the PG is known to upregulate the expression of Halloween genes (*spookier*, *phantom*, *disembodied*, and *shadow*) responsible for ecdysone biosynthesis. In particular, the *shade* gene product is required for the generation of active hormone (20E) from ecdysone in peripheral tissues (Fig. 4B) (McBrayer et al. 2007; Shimell et al. 2018; Christensen et al. 2020). We analyzed the Halloween genes transcript level in *Nup107* depleted larvae and observed a significant downregulation for each Halloween quartet gene mentioned earlier. (Fig. 4C-G; Supplemental Fig. S8B-F). Further, the level of the *shade* gene required for converting precursor ecdysone to active 20E was also reduced twofold in *Nup107*-depleted larvae.

Exogenous supplementation of 20E rescued the EcR localization

The observed correlation between the expression levels of ecdysone biosynthetic genes and reduced levels of 20E strongly suggests a link between the diminished availability of 20E and active 20E-EcR complex formation and nuclear translocation. Interestingly, it has been demonstrated that exogenous ecdysone supplementation through larval food can rescue pupariation blocks resulting from ecdysone deficiency (Garen et al. 1977; Ou et al. 2016; Shimell et al. 2018). We probed the same in *Nup107* depletion conditions and provided exogenous ecdysone to *Nup107*-depleted larvae by feeding them with a diet enriched with 20-hydroxyecdysone (0.2 mg/ml). However, administering 20E to *Nup107* depleted larvae significantly (70-80%) alleviated the developmental arrest, and the onset of pupariation was comparable to the control (Supplemental Table S1). Although, none of the pupae could eventually eclose successfully. We asked if nuclear translocation of EcR can also be rescued by exogenous supplementation of 20E. We noticed a complete EcR nuclear translocation rescue in ubiquitous and PG-specific *Nup107* depleted salivary glands of late third instar larva incubated with 20E. Notably, incubation in control S2 media alone did not impact EcR localization in any genotype (Fig. 5 A-F''; Supplemental Fig. S9)

The exogenous supplementation of 20E leads to active 20E-EcR complex formation as mRNA levels of the *Eip75* and *Eip74EF* target genes are rescued significantly (Fig. 5G, H). Overall, these findings highlight the important regulatory function of Nup107 in the ecdysone signaling pathway.

***Torso* is an effector of *Nup107*-regulated functions in metamorphosis**

Next, we explored the mechanism of Nup107-driven regulation of 20E levels and metamorphosis. Receptor tyrosine kinase family of cell surface receptors signal by binding to ligands (growth

factors and hormones) and participate in metabolism, cell growth, and development. Among these RTKs, the Torso, belonging to the platelet-derived growth factor receptor (PDGFR) class, plays a significant role during metamorphosis by serving as a receptor for the neuropeptide PTTH in the *Drosophila* brain (Sopko and Perrimon 2013).

During post-blastoderm stages of *Drosophila*, PTTH serves as the ligand for the Torso receptor. Functional engagement of PTTH-Torso activates the MAP kinase pathway, involving components of Ras, Raf, MEK, and extracellular signal-regulated kinase (ERK), thereby initiating metamorphosis (Fig. 6A). The *torso* knockdown in the prothoracic glands resulted in the developmental arrest phenotype synonymous to what we have observed with *Nup107* knockdown. Feeding 20E to *torso*-depleted larvae completely rescued developmental delay and normal growth phenotypes (Rewitz et al. 2009). Surprisingly, the *torso* levels decreased significantly (~ four-fold) when *Nup107* was depleted ubiquitously using *Actin5C-GAL4* (Fig. 6B). The phenotypic similarity between *Nup107* and *torso* depletion scenarios and diminished *torso* level upon *Nup107* depletion prompted us to investigate whether *torso* is an effector of Nup107.

We probed the possibility of *Nup107* phenotype rescue with *torso* and ras^{V12} overexpression ubiquitously or in PG. Overexpression of either *torso* or ras^{V12} in *Nup107* depleted background completely rescued the pupariation defects, although with slower kinetics (Fig. 6C-C'; Supplemental Fig. S10A). The *torso* overexpression mediated rescue is specific as overexpression of *Egfr* and *Usp* in *Nup107* depletion background could not rescue the pupariation defects (data not shown). The remarkable rescue demonstrated by *torso* overexpression prompted us to analyze the status of EcR nuclear translocation, ecdysone biosynthesis, and ecdysone-inducible gene expression. The efficient nuclear translocation of EcR, the rescue of ecdysone biosynthesis gene (*spookier*, *phantom*, *disembodied*, and *shadow*), and ecdysone target genes *Eip75A* and *Eip74EF*

indicated that *torso* could efficiently rescue *Nup107* phenotypes to control levels (Fig. 6D-Q; Supplemental Fig. S10B-E).

These observations suggest that the *torso* is a downstream effector of Nup107 functions, and torso-dependent signaling, responsible for 20E synthesis in PG and metamorphosis, is regulated by Nup107 levels.

Discussion

The Nuclear Pore Complex (NPC) is a vital multi-protein assembly facilitating molecular traffic between the nucleus and cytoplasm. The Nup107 complex, a key component of NPC outer rings, acts as a structural scaffold and docking site for other nucleoporins (Hoelz et al. 2016; Lin and Hoelz 2019). Apart from their importance in mRNA export and cell division at the cellular level, the Y-complex nucleoporin, Nup107, when mutated, correlates with developmental abnormalities, microcephaly, and nephrotic syndrome (Zheng et al. 2012; Miyake et al. 2015). In several human cancer types, Nup107 exhibits high expression and serves as a biomarker for hepatocellular carcinoma. A strong structural and functional conservation between human and *Drosophila* Nup107 proteins allows *Drosophila* to be used to model Nup107-related human diseases (Weinberg-Shukron et al. 2015; Shore et al. 2022). Here, we found that Nup107 is essential for developmental transitions in *Drosophila*, as reduced Nup107 levels induce larval arrest and a delayed pupariation (Fig. 1). The foraging third instar larva must acquire a critical weight and sufficient energy stores before it can metamorphose into a non-feeding pupa, molting into a healthy adult. The neuroendocrine Prothoracicotropic hormone activates the Torso receptor to induce a surge in ecdysone synthesis, causing larval to pupal transition (Christensen et al. 2020; Hao et al. 2021; Luo et al. 2024).

Previous studies have shown that elevated ecdysone levels after the third instar larval stage trigger the translocation of the heterodimeric ecdysone receptor [in complex with Ultraspiracle (Usp)] to the nucleus, where it interacts with target DNA and induces pupariation (Johnston et al. 2011). The delayed pupariation we noticed in *Nup107* RNAi accordingly correlated well with perturbed EcR nuclear translocation affecting metamorphosis from third instar larval to pupal stage (Fig. 2). The marked absence of EcR from the nucleus strongly indicates a potential defect in the ecdysone signaling pathway. The observation of EcR mislocalization in *Nup107* RNAi highlights a critical observation of our study, pointing towards an essential regulatory role for Nup107 in ecdysone signaling. Translocation of nuclear receptor proteins from the cytoplasm to the nucleus is a crucial step for transcriptional activation. The cytoplasmic filament Nup, Nup358, plays a vital role in the nuclear import of Met (juvenile hormone receptor) along with Hsp83 (He et al. 2017) to help maintain the larval stages of development. In contrast, we observe that Nup107 is dispensable for the nuclear transport of EcR in target cells. However, the reduced Nup107 levels in the ecdysone-producing prothoracic gland affect the biosynthesis of ecdysone by inducing a reduction in levels of genes involved in ecdysone biosynthesis. Consequently, ecdysone titer is low, the expression levels of ecdysone-inducible genes *Eip75A* and *Eip74EF* are diminished, and larva-to-pupa transition is delayed (Fig 3, 4). In concurrence, reports suggest that a low level of ecdysone disrupts the pupariation process, leading to a halt in insect development (Christensen et al. 2020; Cruz et al. 2020). However, it remains unclear whether Nup107 plays a direct role in ecdysone biosynthesis or if it functions as a regulator of this process.

Insect metamorphosis is regulated by various signaling pathways, where the RTK pathway plays a critical role in associated developmental processes. Notably, Torso signaling is essential for embryonic development and metamorphosis in *Drosophila*. The receptor expression level impacts

the signaling output: high receptor levels trigger a robust and transient signal, while lower levels result in a weaker, sustained signal (Jenni et al. 2015; Konogami et al. 2016). Knockdown of the *torso* in the prothoracic gland leads to reduced ecdysone levels and delayed pupariation (Rewitz et al. 2009), a phenomenon mirroring the defects we observed with *Nup107* knockdown. Interestingly, we observed a decrease in *torso* level upon *Nup107* depletion, suggesting an essential upstream role for Nup107 in regulating RTK pathway activation-dependent *Drosophila* metamorphosis. Moreover, the *torso* RNAi larva has an enlarged body size, a phenotype not observed in the *Nup107* knockdown. In contrast, *Nup107* RNAi larval tissues (salivary glands, brain complex, and prothoracic gland) are significantly smaller in size (Supplemental Fig. S3, S7), suggesting a strong regulatory role for *Nup107* in metamorphosis, adding new dimensions to already known functions of the Y-complex members.

The developmental delays observed in *Nup107* knockdown larvae can be restored by exogenous supplementation of 20E, suggesting that Nup107 can modulate directly or indirectly the Torso receptor for ecdysone production and developmental regulation. Accordingly, we could successfully rescue developmental delays to normal levels by ubiquitous and PG-specific *torso* overexpression. Perhaps overexpression of any of the torso pathway molecules can rescue the *Nup107* developmental delay phenotypes, and the Ras-GTPase, being one of the molecules, has been explored in this regard (Cruz et al. 2020). In concurrence, the oncogenic *ras* mutant (ras^{V12}) overexpression in the *Nup107* knockdown background alleviated the developmental delays (Fig. 6).

Our findings indicate that Nup107 influences pupariation timing by regulating the torso levels, signaling, and ecdysone biosynthesis (Fig 7). Previous research has shown that nuclear pore complexes (NPCs) are essential for maintaining global genome organization and regulating gene

expression (Capelson et al. 2010a; Capelson et al. 2010b; Iglesias et al. 2020). Particularly, Nup107 interacts with chromatin and targets active gene domains to regulate gene expression (Gozalo et al., 2020). Thus, Nup107 exerting its effects on *torso* transcription is the primary regulatory event in the *Drosophila* metamorphosis. Since *torso* overexpression rescues the developmental arrest phenotype and availability of ligands, PTTH may not be affected by the Nup107. It is thus crucial to understand the underlying mechanism of *torso* expression. The whole genome transcriptomics from PG can help shed more light on the regulatory roles of Nup107. This information will offer valuable insights into how nucleoporins regulate gene expression and serve as a model for elucidating how they govern the temporal specificity of developmental processes in organisms. This will also help establish a link between Nup107, the PTTH-PG axis, and the regulation of maturation timing. Thus, our study further highlights the need to explore the interactions of Y-complex Nups and the modulation of other crucial players of these coordination mechanisms in developmental transition.

Material and Methods

Fly stocks and genetics:

Experimental *Drosophila melanogaster* stocks were reared on a standard cornmeal diet (Nutri-Fly Bloomington formulation) under controlled conditions of 25 °C and 60% relative humidity unless otherwise specified. Fly lines used in this study were sourced from the Bloomington *Drosophila* Stock Centre (BDSC) at Indiana University or from the Vienna *Drosophila* Resource Center (VDRC), which are listed in Supplemental Table S3. The UAS-GFP lines were received as a gift from Dr. Varun Chaudhary (IISER Bhopal, India). Control groups were generated through crosses between the driver line and w^{1118} flies. For RNA interference (RNAi) experiments, crosses were maintained at 29 °C to optimize GAL4 expression. The $Nup107^{GD}$ line, in conjunction with *Actin5C-GAL4*, was specifically cultivated at 23 °C to generate third-instar larvae for experimental purposes.

Transgenic fly generation:

In the generation of transgenic flies containing gRNA, we employed a systematic approach. The online tool available at http://targetfinder.flycrispr.neuro.brown.edu was used for the initial sgRNA design, ensuring zero predicted off-targets. Subsequently, we utilized an additional tool available at https://www.flyrnai.org/evaluateCrispr/ to evaluate and score the predicted efficiency of sgRNAs in the targeted region. The most efficient sgRNAs, demonstrating high specificity with no predicted off-targets, were selected and cloned into the pCFD4 vector. The Fly Facility services at the Centre for Cellular and Molecular Platforms, National Center for Biological Sciences (C-CAMP-NCBS), Bangalore, India, were utilized to clone and generate transgenic flies. Primer sequences employed in this study can be found in Supplemental Table S2.

CRISPR –Cas9 mediated mutant Generation:

Virgin nanos.Cas9 (#54591) flies were crossed with males of gRNA transgenic lines, and approximately 10 F1 progeny males were crossed with balancer flies specific for the gene of interest. A single-line cross was established using the F2 progeny to assess the deletion of *nup107*. Subsequently, F3 progeny were subjected to nested PCR to confirm deletions. Positive individuals were further tested for the presence of gRNA and Cas9 transgenes, and flies lacking both were propagated into stocks.

Genomic DNA Isolation:

Approximately ten flies were homogenized in 250 µL of solution A, comprising 0.1 M Tris-HCl, pH 9.0, 0.1 M EDTA, and 1% SDS, supplemented with Proteinase-K. The homogenate was incubated at 70 °C for 30 min. Subsequently, 35 µL of 8 M potassium acetate was added, mixed gently without vortexing, and incubated on ice for 30 min. The homogenate was then centrifuged at 13,000 rpm at 4 °C for 15 min, and the supernatant was carefully collected without disturbing precipitates or the interphase. 150 µL of Isopropanol was added to the supernatant and incubated on ice for 15 min. After centrifugation at 13,000 rpm for 5 min, the supernatant was discarded, and the pellet was washed with 1 mL of 70% ethanol by centrifuging at 13,000 rpm for 5 min. The supernatant was again discarded, and the pellet was dried at 55 °C until the ethanol evaporated. Finally, the pellet was resuspended in 50 µL of Tris-EDTA buffer and incubated at 37 °C.

Nested PCR:

Nested PCR was employed to assess the presence of deletions in flies, utilizing genomic DNA as the template. 1 µL of DNA was used for the initial PCR with an outer set of primers (Supplemental Table S2). Following this, 1 µL of the initial PCR product was employed for a subsequent PCR

with an inner set of primers. The resulting PCR products were then resolved on 0.8% agarose gel to visualize the desired bands indicative of deletions.

Measurement of developmental timing and pupariation:

Flies were permitted to lay eggs for 3 hours on agar plates supplemented with yeast, synchronizing the larvae. Newly hatched L1 larvae were then collected and transferred to vials. Pupariation times and dates were recorded daily during the light cycle. Data from 8-10 vials were aggregated, organized by pupariation time and cumulative percentage pupariation, and analyzed using Microsoft Excel.

Antibody generation and western blotting:

To generate antibodies against *Drosophila Nup107* (CG6743), the N-terminal 210 amino acids, recognized as the most unique and antigenic region, were sub-cloned into the modified tag-less pET28a(+) vector, pET28a(+)-JK vector. The protein was expressed in *Escherichia coli* BL21 (DE3) cells, induced with 200 μM IPTG (Sigma), and incubated at 30 °C for 4 hours. Following cell pelleting, the pellet was resuspended in lysis buffer (50 mM Tris pH 8.0, 1 mM EDTA, and 25% Sucrose) with 1× protease inhibitor mixture (Roche Applied Science), and lysozyme (from 50 mg/mL stock) was added to facilitate bacterial lysis. After sonication and centrifugation, the pellet was successively resuspended in inclusion body buffer I (20 mM Tris pH 8.0, 0.2 M NaCl, 1% Sodium deoxycholate, and 2 mM EGTA) and buffer II (10 mM Tris pH 8.0, 0.25% Sodium deoxycholate and 1 mM EGTA) and centrifuged. This process was repeated three times within inclusion body buffer II, and the final pellet was dissolved in 8 M Urea buffer (10 mM Tris-HCl pH 8.0, 8 M Urea, 0.1 mM NaN_3, and 1 mM EGTA), diluted to 6 M Urea, and centrifuged. The supernatant was loaded onto SDS-PAGE, and the desired band was cut for protein elution. Rabbit

polyclonal antibodies against Nup107 were generated at Bio Bharati Life Sciences Pvt. Ltd., Kolkata, West Bengal, India. The antibodies obtained were subjected to affinity purification. The purification involved the chemical cross-linking of purified antigens to N-hydroxy succinimidyl-Sepharose beads (Sigma). The elution process was carried out under low pH conditions, followed by neutralization. Subsequently, the eluted antibodies were dialyzed against phosphate-buffered saline (PBS) overnight at 4 °C to remove any remaining impurities and optimize their stability and functionality for subsequent experimental use.

Larval brain complexes from third-instar larvae were dissected, lysed in Laemmli buffer, and resolved on 8% SDS-PAGE. Two equivalent head complexes were loaded per well. After transfer to a polyvinylidene difluoride membrane, blocking was performed with 5% fat-free milk. The membrane was then incubated with polyclonal anti-Nup107 antibody (1:500) and anti-α-tubulin (DSHB, 12G10) (1:5000) at 4 °C overnight. Following three washes with TBS-T buffer (20 mM Tris-HCl pH 7.5, 150 mM NaCl, 0.1% Tween-20), the membrane was incubated with secondary antibodies, Alexa-Fluor Plus 680 (Invitrogen #A32734) and Alexa-Fluor Plus 800 (Invitrogen #A32730). Following incubation with secondary antibodies, the membrane was washed three times for 10 minutes each with Tris-buffered saline containing Tween-20 (TBS-T) to remove unbound antibodies. The washed membrane was then subjected to imaging using the Li-Cor IR system (Model: 9120), allowing for the visualization and analysis of the protein bands on the membrane.

Immunostaining:

For immunostaining *Drosophila* salivary glands, primarily the protocol reported by Mehta et al., 2021 was followed. The larvae were dissected in cold phosphate-buffered saline (PBS) to isolate salivary glands. Glands underwent pre-extraction with 1% PBST (PBS + 1% Triton X-100), then

fixation in freshly prepared 4% formaldehyde for 30 minutes at room temperature. Subsequently, the glands were thoroughly washed with 0.3% PBST (0.3% Triton X-100 containing PBS). Blocking was performed for 1 h with 5% normal goat serum (#005-000-001, The Jackson Laboratory, USA). The glands were stained with the following primary antibodies: anti-Nup107 (1:100), mAb414 (1:500, Bio-legend) and anti-EcR (1:20, DDA2.7, DSHB) overnight at 4 °C. Tissues were washed three times with 0.3% PBST (PBS + 0.3% Triton X-100), followed by incubation with secondary antibodies: anti-rabbit Alexa Fluor 488 (1:800, #A11034, Thermo Fisher Scientific), anti-rabbit Alexa Fluor 568 (1:800, #A11036, Thermo Fisher Scientific), anti-mouse Alexa Fluor 488 (1:800, #A11029, Thermo Fisher Scientific), anti-mouse Alexa Fluor 568 (1:800, #A11004, Thermo Fisher Scientific), and anti-rabbit Alexa Fluor 647 (1:800, Thermo Fisher Scientific). Following secondary antibody incubation, tissues were washed three times with 0.3% PBST (PBS + 0.2% Triton X-100) and mounted with DAPI-containing Fluoroshield (#F6057, Sigma). The same protocol was followed for staining of the Brain complex and prothoracic gland.

Intensity quantification:

Images were acquired using an Olympus Confocal Laser Scanning Microscope FV3000. Subsequent image processing was conducted using the Fiji software, and signal intensities were averaged using GraphPad software (Prism). To quantify the EcR nuclear to cytoplasmic ratio, three distinct regions of interest (ROI) were designated per nucleus and its surrounding cytoplasm. Fiji software measured the average intensity in each ROI, and the mean of these intensities was determined per nucleus and its adjacent cytoplasm. The final graph depicts the ratio of the mean intensities observed in the nucleus to that in the cytoplasm. All experiments were conducted with a minimum of three independent replicates.

Quantitative RT-PCR:

Total RNA was extracted from various genotypes (control, ubiquitously depleted *Nup107*, and prothoracic gland-specific depletion of *Nup107*) of whole late third instar larvae utilizing the total tissue RNA isolation kit (Favorgen Biotech). One microgram of total RNA was employed for cDNA synthesis with the iScript cDNA synthesis kit (Bio-Rad). The resulting cDNA was diluted fivefold, and 1 µL from each genotype was utilized as a template. RT-PCR was conducted using SYBR Green PCR master mix on an Applied Biosystems QuantStudio 3 Real-Time PCR System. The Rpl69 gene served as the control, and relative transcript levels were determined using the CT value ($2^{-\Delta\Delta CT}$). Differences in gene expression were analyzed using Student's t-test, with a p-value < 0.05 considered significant. The primers used are detailed in the Supplemental Table S2. The resultant graph illustrated the fold change in gene expression, plotted using GraphPad software (Prism).

20-hydroxyecdysone (20E) level measurements:

Three biological replicates of 25 mg larvae from each genotype were collected at the specified times after egg laying (AEL). The larvae were washed, dried, and weighed before being flash-frozen on dry ice and stored at -80 °C. Ecdysone extraction was done by thoroughly homogenizing the frozen samples in 300 µL ice-cold methanol with a plastic pestle. After centrifugation at 17,000 x g for 10 minutes, the supernatant was divided into two Eppendorf tubes containing approximately 150 µL supernatant. Methanol from both tubes was evaporated in a vacuum centrifuge for 60 minutes, and the resulting pellets were redissolved by adding 200 µL Enzyme Immunoassay (EIA) buffer to one of the tubes. After vortexing, the same 200 µL EIA buffer was transferred to the second tube, followed by another round of vortexing. The Enzyme-Linked Immunosorbent Assay

(ELISA) was performed using a 20-hydroxyecdysone ELISA kit (#EIAHYD) from ThermoFisher Scientific.

20E Rescue Experiment:

20-hydroxyecdysone (Sigma, H5142) was dissolved in ethanol to achieve a 5 mg/mL concentration. Salivary glands from third instar larvae of different genotypes were extracted and then incubated for 6 hours in Schneider's S2 media with 50 μM 20E. After the incubation, the glands underwent procedures for immunostaining and RNA extraction.

To facilitate the rescue of the larvae through feeding, 30-third instar larvae, *Nup107* depleted larvae cultured at 29 °C incubator, were first washed with water. They were then transferred to vials containing either 20E (at a final concentration of 0.2 mg/mL) or 95% ethanol (in the same amount as the 20E). Once the larvae were added to the vials, these were returned to the 29 °C incubator and observed for pupariation, recording the time of this developmental stage.

Competing interest statement

The authors declare no competing interests.

Acknowledgment

We thank the Bloomington *Drosophila* Stock Centre (BDSC) and Vienna *Drosophila* Resource Centre (VDRC) for generously providing the fly lines crucial for this study. Special recognition is given to Bio Bharati Life Sciences Pvt. Ltd., Kolkata, India, for their significant contribution to antibody generation and the Developmental Studies Hybridoma Bank (DSHB) for supplying antibodies. Furthermore, our sincere thanks go to C-CAMP Bengaluru for their instrumental role in generating the transgenic fly. BioRender was used to create models wherever necessary. The

Indian Institute of Science Education and Research Bhopal Central Instrumentation Facility is acknowledged for its valuable support in DNA sequencing and facilitating access to confocal microscopes. We acknowledge critical discussions and timely experimental suggestions extended by Mr, Pradyumna Ajit Joshi. This work was supported by the Science and Engineering Research Board grant no. CRG/2020/000496 provided to RKM.

Author Contribution

JK and RKM conceptualized the project and the experimental plan and wrote the manuscript. JK performed all experiments and analyzed data. RKM provided intellectual support in data analysis and secured funding for the project.

References

Bai SW, Rouquette J, Umeda M, Faigle W, Loew D, Sazer S, Doye V. 2004. The fission yeast Nup107-120 complex functionally interacts with the small GTPase Ran/Spi1 and is required for mRNA export, nuclear pore distribution, and proper cell division. *Mol Cell Biol* **24**: 6379-6392.

Boehmer T, Enninga J, Dales S, Blobel G, Zhong H. 2003. Depletion of a single nucleoporin, Nup107, prevents the assembly of a subset of nucleoporins into the nuclear pore complex. *Proc Natl Acad Sci U S A* **100**: 981-985.

Capelson M, Doucet C, Hetzer MW. 2010a. Nuclear pore complexes: guardians of the nuclear genome. *Cold Spring Harb Symp Quant Biol* **75**: 585-597.

Capelson M, Liang Y, Schulte R, Mair W, Wagner U, Hetzer MW. 2010b. Chromatin-bound nuclear pore components regulate gene expression in higher eukaryotes. *Cell* **140**: 372-383.

Chen X, Xu L. 2010. Specific nucleoporin requirement for Smad nuclear translocation. *Mol Cell Biol* **30**: 4022-4034.

Christensen CF, Koyama T, Nagy S, Danielsen ET, Texada MJ, Halberg KA, Rewitz K. 2020. Ecdysone-dependent feedback regulation of prothoracicotropic hormone controls the timing of developmental maturation. *Development* **147**.

Cronauer MV, Braun S, Tremmel C, Kroncke KD, Spindler-Barth M. 2007. Nuclear localization and DNA binding of ecdysone receptor and ultraspiracle. *Arch Insect Biochem Physiol* **65**: 125-133.

Cronshaw JM, Krutchinsky AN, Zhang W, Chait BT, Matunis MJ. 2002. Proteomic analysis of the mammalian nuclear pore complex. *J Cell Biol* **158**: 915-927.

Cruz J, Martin D, Franch-Marro X. 2020. Egfr Signaling Is a Major Regulator of Ecdysone Biosynthesis in the Drosophila Prothoracic Gland. *Curr Biol* **30**: 1547-1554 e1544.

D'Angelo MA, Hetzer MW. 2008. Structure, dynamics and function of nuclear pore complexes. *Trends Cell Biol* **18**: 456-466.

Garen A, Kauvar L, Lepesant JA. 1977. Roles of ecdysone in Drosophila development. *Proc Natl Acad Sci U S A***74**: 5099-5103.

Gozalo A, Duke A, Lan Y, Pascual-Garcia P, Talamas JA, Nguyen SC, Shah PP, Jain R, Joyce EF, Capelson M. 2020. Core Components of the Nuclear Pore Bind Distinct States of Chromatin and Contribute to Polycomb Repression. *Mol Cell***77**: 67-81 e67.

Hao S, Gestrich JY, Zhang X, Xu M, Wang X, Liu L, Wei H. 2021. Neurotransmitters Affect Larval Development by Regulating the Activity of Prothoracicotropic Hormone-Releasing Neurons in Drosophila melanogaster. *Front Neurosci***15**: 653858.

Hayashi D, Tanabe K, Katsube H, Inoue YH. 2016. B-type nuclear lamin and the nuclear pore complex Nup107-160 influences maintenance of the spindle envelope required for cytokinesis in Drosophila male meiosis. *Biol Open***5**: 1011-1021.

He Q, Zhang Y, Zhang X, Xu D, Dong W, Li S, Wu R. 2017. Nucleoporin Nup358 facilitates nuclear import of Methoprene-tolerant (Met) in an importin beta- and Hsp83-dependent manner. *Insect Biochem Mol Biol***81**: 10-18.

Hetzer MW, Wente SR. 2009. Border control at the nucleus: biogenesis and organization of the nuclear membrane and pore complexes. *Dev Cell***17**: 606-616.

Hoelz A, Glavy JS, Beck M. 2016. Toward the atomic structure of the nuclear pore complex: when top down meets bottom up. *Nat Struct Mol Biol***23**: 624-630.

Iglesias N, Paulo JA, Tatarakis A, Wang X, Edwards AL, Bhanu NV, Garcia BA, Haas W, Gygi SP, Moazed D. 2020. Native Chromatin Proteomics Reveals a Role for Specific Nucleoporins in Heterochromatin Organization and Maintenance. *Mol Cell***77**: 51-66 e58.

Jenni S, Goyal Y, von Grotthuss M, Shvartsman SY, Klein DE. 2015. Structural Basis of Neurohormone Perception by the Receptor Tyrosine Kinase Torso. *Mol Cell***60**: 941-952.

Johnson TK, Crossman T, Foote KA, Henstridge MA, Saligari MJ, Forbes Beadle L, Herr A, Whisstock JC, Warr CG. 2013. Torso-like functions independently of Torso to regulate Drosophila growth and developmental timing. *Proc Natl Acad Sci U S A***110**: 14688-14692.

Johnston DM, Sedkov Y, Petruk S, Riley KM, Fujioka M, Jaynes JB, Mazo A. 2011. Ecdysone- and NO-mediated gene regulation by competing EcR/Usp and E75A nuclear receptors during Drosophila development. *Mol Cell***44**: 51-61.

Kalverda B, Pickersgill H, Shloma VV, Fornerod M. 2010. Nucleoporins directly stimulate expression of developmental and cell-cycle genes inside the nucleoplasm. *Cell***140**: 360-371.

Kannangara JR, Mirth CK, Warr CG. 2021. Regulation of ecdysone production in Drosophila by neuropeptides and peptide hormones. *Open Biol***11**: 200373.

Kim SY, Kang HT, Choi HR, Park SC. 2010. Reduction of Nup107 attenuates the growth factor signaling in the senescent cells. *Biochem Biophys Res Commun***401**: 131-136.

Konogami T, Yang Y, Ogihara MH, Hikiba J, Kataoka H, Saito K. 2016. Ligand-dependent responses of the silkworm prothoracicotropic hormone receptor, Torso, are maintained by unusual intermolecular disulfide bridges in the transmembrane region. *Sci Rep***6**: 22437.

Kozlova T, Thummel CS. 2002. Spatial patterns of ecdysteroid receptor activation during the onset of Drosophila metamorphosis. *Development***129**: 1739-1750.

Kuhn TM, Pascual-Garcia P, Gozalo A, Little SC, Capelson M. 2019. Chromatin targeting of nuclear pore proteins induces chromatin decondensation. *J Cell Biol***218**: 2945-2961.

Lenaerts C, Marchal E, Peeters P, Vanden Broeck J. 2019. The ecdysone receptor complex is essential for the reproductive success in the female desert locust, Schistocerca gregaria. *Sci Rep***9**: 15.

Lin DH, Hoelz A. 2019. The Structure of the Nuclear Pore Complex (An Update). *Annu Rev Biochem***88**: 725-783.

Luo X, Zhang J, Zhang C, Zhou N. 2024. PTTH-Torso Signaling System Controls Developmental Timing, Body Size, and Reproduction through Regulating Ecdysone Homeostasis in the Brown Planthopper, Nilaparvata lugens. *Int J Mol Sci***25**.

McBrayer Z, Ono H, Shimell M, Parvy JP, Beckstead RB, Warren JT, Thummel CS, Dauphin-Villemant C, Gilbert LI, O'Connor MB. 2007. Prothoracicotropic hormone regulates developmental timing and body size in Drosophila. *Dev Cell***13**: 857-871.

Mehta SJK, Kumar V, Mishra RK. 2020. Drosophila ELYS regulates Dorsal dynamics during development. *J Biol Chem***295**: 2421-2437.

Mehta SJK, Joshi PA, Mishra RK, 2021. Molecular and Phenotypic Characterization Following RNAi Mediated Knockdown in Drosophila. Bio Protoc 11: e3924.

Mishra RK, Chakraborty P, Arnaoutov A, Fontoura BM, Dasso M. 2010. The Nup107-160 complex and gamma-TuRC regulate microtubule polymerization at kinetochores. *Nat Cell Biol***12**: 164-169.

Miyake N, Tsukaguchi H, Koshimizu E, Shono A, Matsunaga S, Shiina M, Mimura Y, Imamura S, Hirose T, Okudela K et al. 2015. Biallelic Mutations in Nuclear Pore Complex Subunit NUP107 Cause Early-Childhood-Onset Steroid-Resistant Nephrotic Syndrome. *Am J Hum Genet***97**: 555-566.

Morchoisne-Bolhy S, Geoffroy MC, Bouhlel IB, Alves A, Auduge N, Baudin X, Van Bortle K, Powers MA, Doye V. 2015. Intranuclear dynamics of the Nup107-160 complex. *Mol Biol Cell***26**: 2343-2356.

Niwa R, Niwa YS. 2014. Enzymes for ecdysteroid biosynthesis: their biological functions in insects and beyond. *Biosci Biotechnol Biochem***78**: 1283-1292.

Ou Q, Zeng J, Yamanaka N, Brakken-Thal C, O'Connor MB, King-Jones K. 2016. The Insect Prothoracic Gland as a Model for Steroid Hormone Biosynthesis and Regulation. *Cell Rep***16**: 247-262.

Rabut G, Doye V, Ellenberg J. 2004a. Mapping the dynamic organization of the nuclear pore complex inside single living cells. *Nat Cell Biol***6**: 1114-1121.

Rabut G, Lenart P, Ellenberg J. 2004b. Dynamics of nuclear pore complex organization through the cell cycle. *Curr Opin Cell Biol***16**: 314-321.

Rewitz KF, Yamanaka N, Gilbert LI, O'Connor MB. 2009. The insect neuropeptide PTTH activates receptor tyrosine kinase torso to initiate metamorphosis. *Science***326**: 1403-1405.

Rewitz KF, Yamanaka N, O'Connor MB. 2013. Developmental checkpoints and feedback circuits time insect maturation. *Curr Top Dev Biol***103**: 1-33.

Rout MP, Aitchison JD, Suprapto A, Hjertaas K, Zhao Y, Chait BT. 2000. The yeast nuclear pore complex: composition, architecture, and transport mechanism. *J Cell Biol***148**: 635-651.

Shimell M, Pan X, Martin FA, Ghosh AC, Leopold P, O'Connor MB, Romero NM. 2018. Prothoracicotropic hormone modulates environmental adaptive plasticity through the control of developmental timing. *Development***145**.

Shore T, Levi T, Kalifa R, Dreifuss A, Rekler D, Weinberg-Shukron A, Nevo Y, Bialistoky T, Moyal V, Gold MY et al. 2022. Nucleoporin107 mediates female sexual differentiation via Dsx. *Elife***11**.

Sopko R, Perrimon N. 2013. Receptor tyrosine kinases in Drosophila development. *Cold Spring Harb Perspect Biol***5**.

Tennessen JM, Thummel CS. 2011. Coordinating growth and maturation - insights from Drosophila. *Curr Biol***21**: R750-757.

Varghese J, Cohen SM. 2007. microRNA miR-14 acts to modulate a positive autoregulatory loop controlling steroid hormone signaling in Drosophila. *Genes Dev***21**: 2277-2282.

Walther TC, Alves A, Pickersgill H, Loiodice I, Hetzer M, Galy V, Hulsmann BB, Kocher T, Wilm M, Allen T et al. 2003. The conserved Nup107-160 complex is critical for nuclear pore complex assembly. *Cell***113**: 195-206.

Weinberg-Shukron A, Renbaum P, Kalifa R, Zeligson S, Ben-Neriah Z, Dreifuss A, Abu-Rayyan A, Maatuk N, Fardian N, Rekler D et al. 2015. A mutation in the nucleoporin-107 gene causes XX gonadal dysgenesis. *J Clin Invest***125**: 4295-4304.

Yamanaka N, Rewitz KF, O'Connor MB. 2013. Ecdysone control of developmental transitions: lessons from Drosophila research. *Annu Rev Entomol* **58**: 497-516.

Zheng X, Yang S, Han Y, Zhao X, Zhao L, Tian T, Tong J, Xu P, Xiong C, Meng A. 2012. Loss of zygotic NUP107 protein causes missing of pharyngeal skeleton and other tissue defects with impaired nuclear pore function in zebrafish embryos. *J Biol Chem* **287**: 38254-38264.

Zuccolo M, Alves A, Galy V, Bolhy S, Formstecher E, Racine V, Sibarita JB, Fukagawa T, Shiekhattar R, Yen T et al. 2007. The human Nup107-160 nuclear pore subcomplex contributes to proper kinetochore functions. *EMBO J* **26**: 1853-1864.

Figures and figure legends

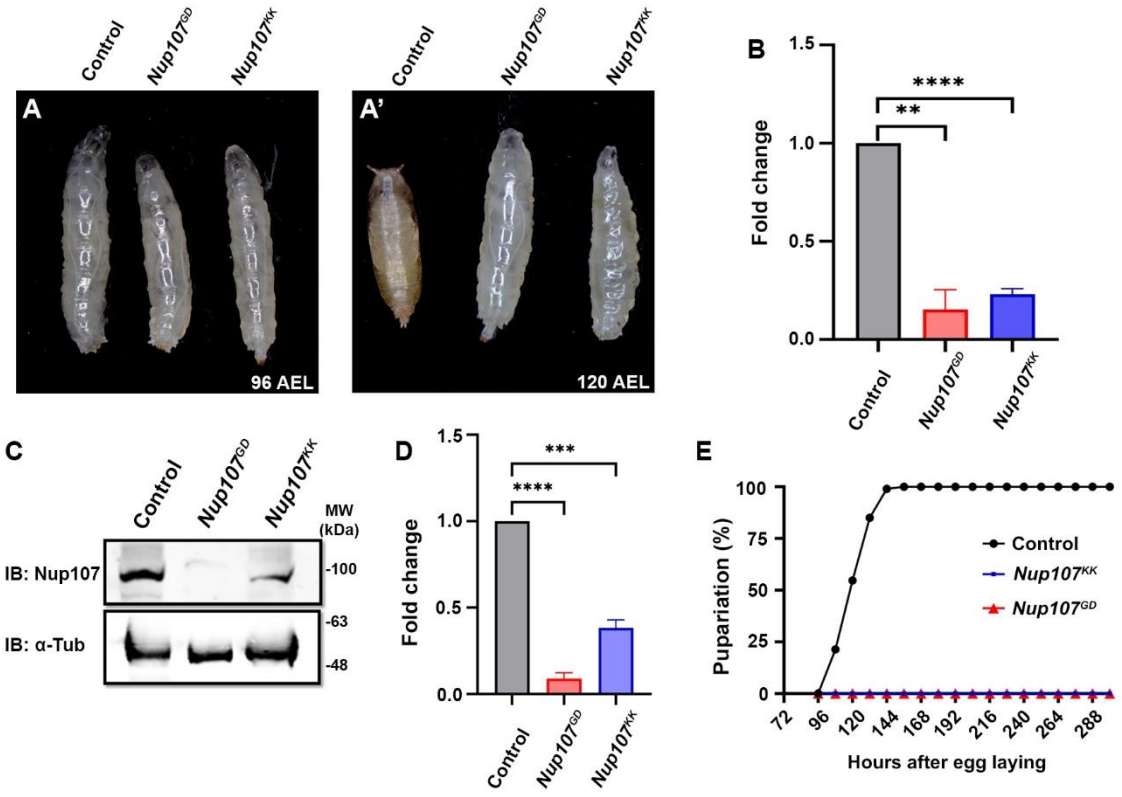

Figure 1. *Nup107* depletion impairs metamorphosis. (A, A') Growth profile of third instar larvae from *Actin5C-Gal4* driven control and *Nup107* knockdowns (*Nup107*^{GD} and *Nup107*^{KK} RNAi lines). (B) Quantitation of *Nup107* knockdown efficiency. Data are represented from at least three independent experiments. Statistical significance was derived from the Student's t-test. Error bars represent SEM. (**) = p <0.001 and (****) = p <0.0001. (C) Detection of Nup107 protein levels in third instar larval brain-complex lysates from control and *Nup107* knockdown. (D) Quantification of Nup107 protein levels seen in (C). Data are represented from at least three independent experiments. Statistical significance was derived from the Student's t-test. Error bars represent SEM. (***) = p <0.0002 and (****) = p <0.0001. (E) Comparison of pupariation profiles of control and *Nup107* knockdown organisms.

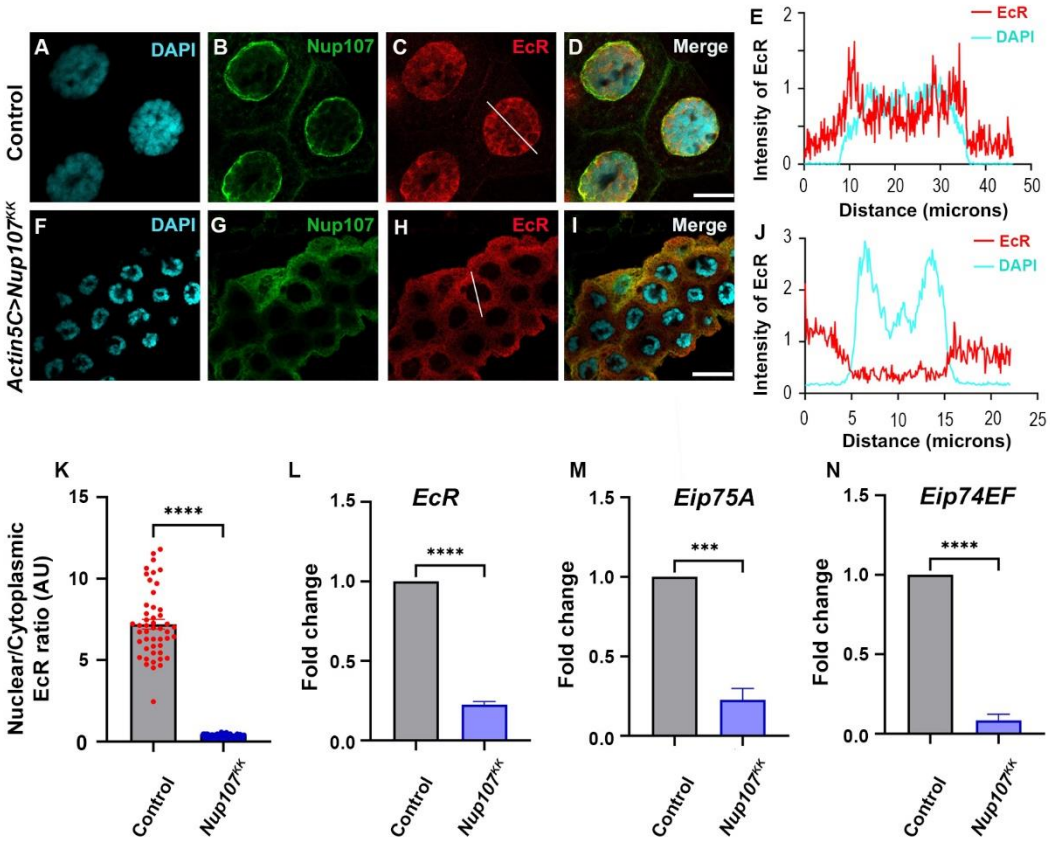

Figure 2. Ubiquitous knockdown of *Nup107* disrupts ecdysone signaling. Staining of third instar larval salivary glands from control (A-D) and ubiquitous *Nup107* knockdown (F-I) with Ecdysone receptor (EcR, red) and Nup107 (green). DNA is stained with DAPI. Scale bars, 20 µm. (E, J) Line scan intensity profile of salivary gland nucleus regions of control and *Nup107* RNAi, respectively. (K) Quantification of nucleo-cytoplasmic ratio of EcR under control and *Nup107* knockdown conditions. At least 45 nuclei were analyzed from 7 to 8 pairs of salivary glands. Statistical significance was derived from the Student's t-test. Error bars represent SEM. (****) = $p < 0.0001$. (L-N) Analysis of ecdysone-inducible genes, *EcR*, *Eip75A*, and *Eip74EF* expression, respectively, at the onset of metamorphosis (late third instar larvae stage). Data are represented

from at least three independent experiments. Statistical significance was derived from the Student's t-test. The error bars represent the SEM. (***) = p <0.0004 and (****) = p <0.0001.

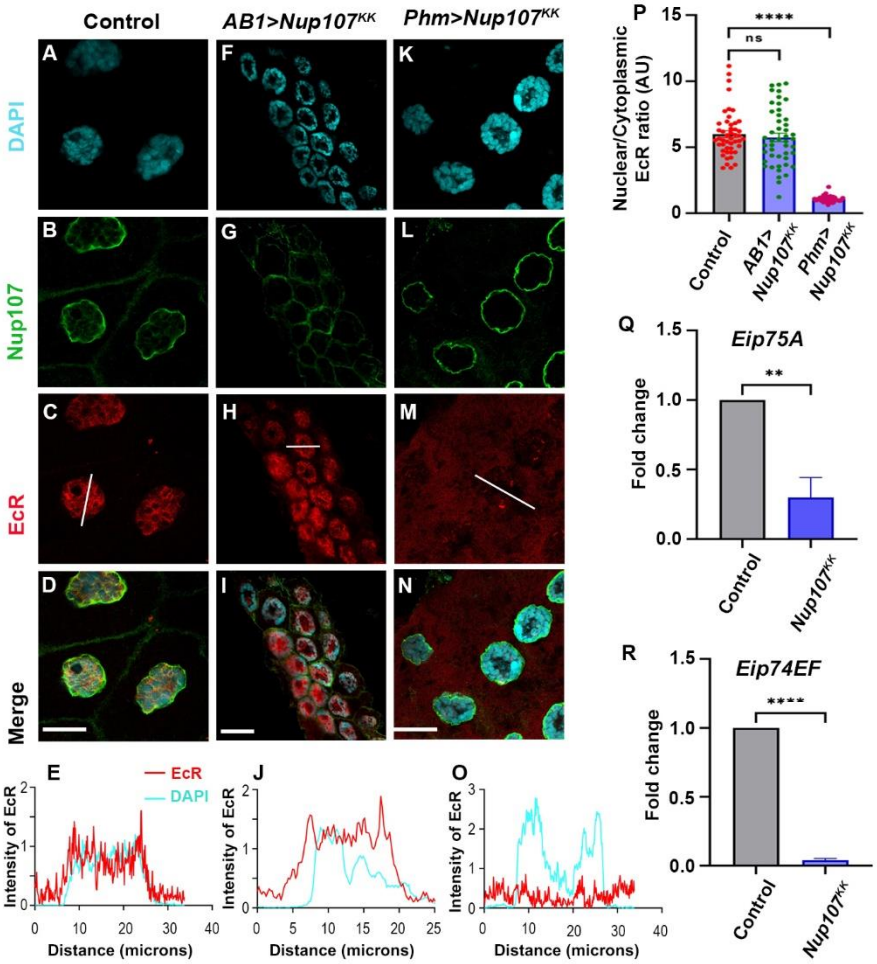

Figure 3. *Nup107* regulates Ecdysone receptor-dependent signaling. Detection of and quantitation of nucleocytoplasmic distribution of EcR (anti-EcR antibody, red) and Nup107 (anti-Nup107 antibody, green) in control (A-E), salivary gland-specific *Nup107* depletion (F-J), and prothoracic gland-specific *Nup107* depletion (K-O) from third instar larval salivary gland nuclei. DNA is stained with DAPI. Scale bars, 20 µm. (P) EcR nucleo-cytoplasmic quantification ratio from the salivary gland and prothoracic gland-specific *Nup107* knockdown, respectively. At least 45 nuclei were analyzed from 7 to 8 pairs of salivary glands. Statistical significance was derived

from the Student's t-test. Error bars represent SEM. (****) = p <0.0001, and ns is non-significant. (Q-R) Quantitation of expression of *Eip75A* and *Eip74EF* ecdysone-inducible genes at the onset of metamorphosis (RNA isolated from late third instar larvae of control and prothoracic gland-specific *Nup107* depletion). Data are represented from at least three independent experiments. Statistical significance was derived from the Student's t-test. Error bars represent SEM. (**) = p <0.008 and (****) = p <0.0001.

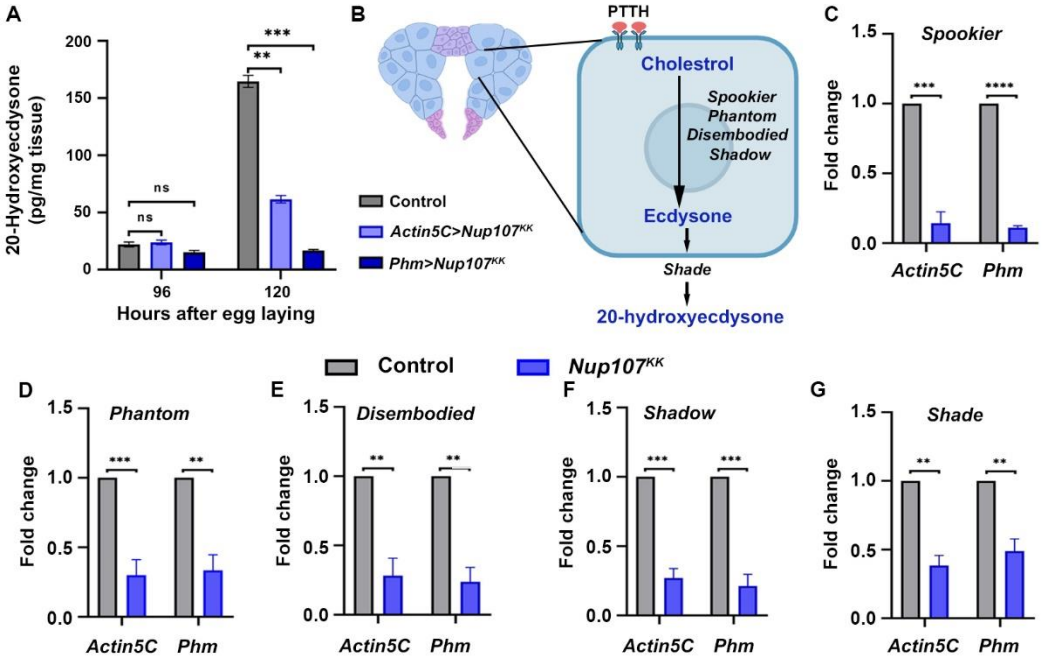

Figure 4. *Nup107* critically regulates the expression of ecdysone-biosynthetic genes. (A) ELISA measurements of whole-body 20-hydroxyecdysone (20E) levels in control, ubiquitous (*Actin5C-Gal4*), and prothoracic gland-specific (*Phm-Gal4*) *Nup107* depletion at 96 and 120 h AEL. Data are represented from at least three independent experiments. Statistical significance was derived from the Student's t-test. Error bars represent SEM. (**) = p <0.0013, (***) = p < 0.0009 and ns is non-significant. (B) Schematic representation of a Prothoracic gland cell showing genes involved in ecdysone biosynthesis from cholesterol. (C-G) Quantification of ecdysone-biosynthetic gene expression levels of *Spookier* (C), *Phantom* (D), *Disembodied* (E), *Shadow* (F), and *Shade* (G) in cDNA isolated from control, and *Nup107* knockdown late third instar larvae. Data are represented from at least three independent experiments. Statistical significance was derived from the Student's t-test. Error bars represent SEM. (**) = p <0.001, (***) = p <0.0005 and, (****) = p <0.0001.

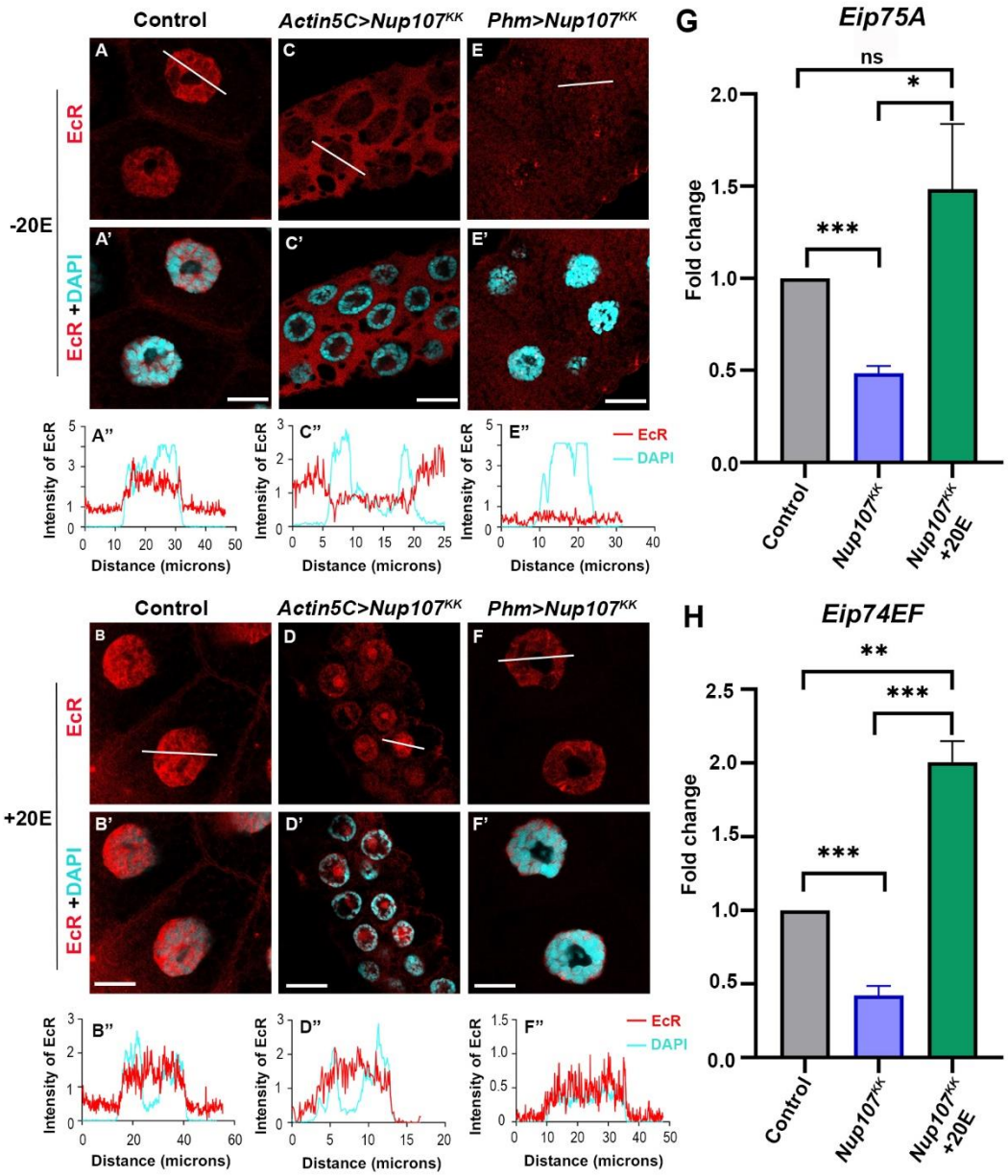

Figure 5. 20E supplementation rescues *Nup107* depletion-specific EcR signaling defects. Visualization of nucleocytoplasmic distribution of EcR (anti-EcR antibody, red) without 20E (-20E) and with 20E (+20E) treatment in larval salivary glands of control (-20E, A-A" and +20E, B-B"), ubiquitous (*Actin5C-Gal4*) *Nup107* knockdown (-20E, C-C" and +20E, D-D"), and prothoracic gland-specific (*Phm-Gal4*) *Nup107* knockdown (-20E, E-E" and +20E, F-F"). DNA is stained with DAPI. Scale bars, 20 µm. (G-H) Comparative quantification of expression ecdysone-

inducible genes *Eip75A* and *Eip74EF* from 20E treated salivary glands. Data are represented from at least three independent experiments. Statistical significance was derived from the Student's t-test. Error bars represent SEM. (*) = $p < 0.02$, (**) = $p < 0.002$, (***) = $p < 0.0008$ and ns is non-significant.

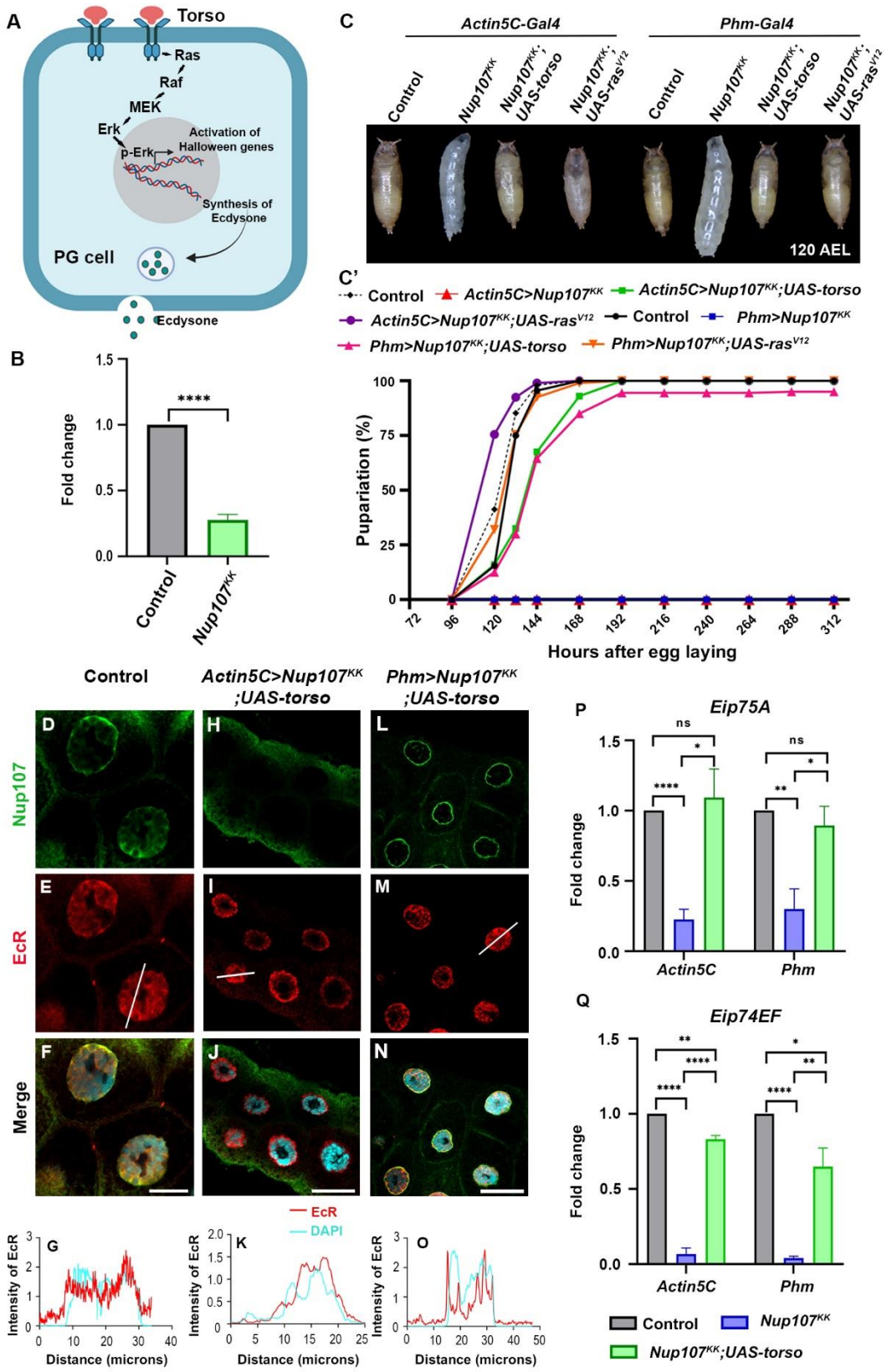
A
Torso
Ras
Raf
MEK
Erk
p-Erk
Activation of Halloween genes
Synthesis of Ecdysone
PG cell
Ecdysone
B
Fold change
****
Control
Nup107KK
C
Actin5C-Gal4
Phm-Gal4
Control
Nup107KK
Nup107KK; UAS-torso
Nup107KK; UAS-rasV12
120 AEL
C'
Control
Actin5C>Nup107KK
Actin5C>Nup107KK;UAS-torso
Actin5C>Nup107KK;UAS-rasV12
Phm>Nup107KK
Phm>Nup107KK;UAS-torso
Phm>Nup107KK;UAS-rasV12
Pupariation (%)
Hours after egg laying
Control
Actin5C>Nup107KK ;UAS-torso
Phm>Nup107KK ;UAS-torso
Nup107
EcR
Merge
Intensity of EcR
Distance (microns)
EcR
DAPI
P
Eip75A
ns
Fold change
Actin5C
Phm
Q
Eip74EF
Control
Nup107KK
Nup107KK;UAS-torso

Figure 6. *Torso* and *Nup107* act synergistically to activate the ecdysone signaling. (A) A model of the Torso pathway and its components. (B) Quantitation of *torso* transcript levels from control and *Nup107* depleted larvae (ubiquitous depletion by using *Actin5C-Gal4*). Data are represented from at least three independent experiments. Statistical significance was derived from the Student's t-test. Error bars represent SEM. (****) = $p < 0.0001$. (C-C') Comparison of pupariation profiles of control, *Nup107* knockdown, and *torso* and ras^{V12} overexpressing rescue organisms. (D-O) Detection of and quantitation of nucleocytoplasmic distribution of EcR (anti-EcR antibody, red) and Nup107 (anti-Nup107 antibody, green) in control (D-G), *torso* overexpressing ubiquitous *Nup107* knockdown (*Actin5C-Gal4>Nup107*^{KK}*; UAS-torso*, H-K) and *torso* overexpressing PG-specific *Nup107* knockdown (*Phm-Gal4>Nup107*^{KK}; *UAS-torso*, L-O) third instar larval salivary gland nuclei. DNA is stained with DAPI. Scale bars, 20 μm. (P-Q) Quantification of expression of *Eip75A* and *Eip74EF* ecdysone-inducible genes, respectively. Data are represented from at least three independent experiments. Statistical significance was derived from the Student's t-test. Error bars represent SEM. (*) = $p < 0.03$, (**) = $p < 0.008$, (****) = $p < 0.0001$ and ns is non-significant.

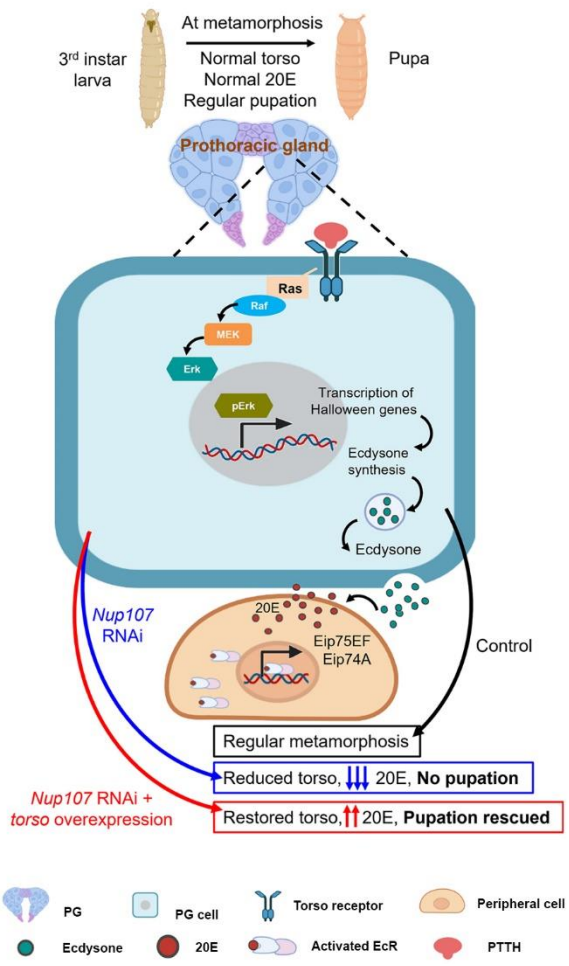

Figure 7. Theoretical Model of Nup107 functions in metamorphosis:

During metamorphosis, the prothoracic gland (PG) responds to prothoracicotropic hormone (PTTH) via Torso receptors. The MAP kinase pathway involving Raf, MEK, and ERK, initiated by Ras, leads to Halloween gene expression responsible for Ecdysone synthesis and release. Ecdysone is converted to active 20-hydroxyecdysone (20E) in peripheral tissues. The binding of 20E to the Ecdysone receptor (EcR) allows EcR nuclear translocation and EcR pathway activation, culminating in target gene expression and facilitating the metamorphic transition. Depleted Nup107 negatively impacts Torso levels and Torso pathway activation, inducing pupariation arrest, which can be rescued by autonomous activation of the Torso pathway.